Chaos, Solitons and Fractals 169 (2023) 113241

Contents lists available at ScienceDirect

Chaos, Solitons and Fractals

journal homepage: www.elsevier.com/locate/chaos

The universal law of the front speed close to the disappearance of bistability

P.J. Aguilera-Rojas [a,*], K. Alfaro-Bittner [b], M.G. Clerc [a], G. González-Cortés [a], R.G. Rojas [c]

[a] Departamento de Física and Millennium Institute for Research in Optics, Facultad de Ciencias Físicas y Matemáticas, Universidad de Chile, Casilla 487-3, Santiago, Chile

[b] Universidad Rey Juan Carlos, Calle Tulipán s/n, 28933 Móstoles, Madrid, Spain

[c] Instituto de Física, Pontificia Universidad Católica de Valparaíso, Casilla 4059, Valparaíso, Chile

ARTICLE INFO

Keywords:
Front propagation
Bifurcation theory
Nonequilibrium system
Liquid crystals

ABSTRACT

Multistable systems present rich dynamical behaviors of interfaces between the different equilibria. Close to the disappearance of bistability, i.e., transition between a bistable to a monostable region, we show that the speed of bistable fronts follows a square root law as a function of the bifurcation parameter. Analytically and numerically, we show this law for different prototype models of bistable systems. Based on a liquid crystal light valve experiment with optical feedback, we investigate the front speed close to the disappearance of bistability. Our results apply both to systems that do or do not follow energy minimization principles. Experimental findings show a quite fair agreement with the theoretical results.

1. Introduction

Macroscopic systems out-of-equilibrium are characterized by the coexistence of different equilibria, *multistability* [1–3]. Depending on the initial conditions, one can observe the different states or solutions composed of these equilibria. Such solutions are characterized by the interface propagation between these domains, which are usually called domain walls, nonlinear wavefronts, or fronts depending on the physical context under study [1–6]. Front dynamics have been observed in diverse fields, such as walls separating magnetic domains, liquid crystal phases, fluidized granular states, chemical reactions, solidification and combustion processes, and populations dynamics, to mention a few. Indeed, fronts propagation is a robust phenomenon ranging from chemistry and biology to physics. In one-dimensional systems, propagative fronts can be regarded as particle-type solutions, i.e., they can be characterized by a set of continuous parameters such as position, core width, and so forth. These dynamical behaviors correspond to nonlinear waves, i.e., the superposition principle is no longer valid, and for different initial conditions, the front propagates with the same shape (profile) and speed [1,6]. Indeed, the propagation and dynamics of fronts depend on the nature of the states (domains) that are being connected. For instance, in the case of a front connecting a stable equilibrium with an unstable one, the stable state usually invades the unstable one [2,5], usually termed FKPP fronts. The combustion, spread of permanent contagious diseases, and freezing of supercooled water are enthralling example of this type of fronts. These types of fronts initially emerged in population dynamics and gene spreads [2]. The wavefront speed is not unique; it depends on the initial conditions and can be determined by the linear dynamics around the unstable equilibrium (pulled fronts) or by the nonlinear saturation around the stable equilibrium (pushed fronts) [5]. If the initial condition is bounded, the system always spread with the minimum speed. Note that the invasion of the unstable state into a stable one has also been reported [7].

The above scenario changes radically when considering fronts connecting two stable states, *bistable fronts* [1,6]. These fronts are characterized by exhibiting a single propagation speed that, in fact, does not depend on the initial conditions. In the case of one-dimensional variational or gradient systems, propagation speed depends on the energy difference between the two equilibria [8,9]. Hence, the more stable state invades the less stable one. Then, one expects a point in the parameter space where the relative energy between the two equilibria is equal, *the Maxwell point* [10], at which the front is motionless. In his pioneering work, Pomeau proposes a universal semi-implicit formula for the front speed [8], which accounts for the energy difference between states. Analytical results are only accessible close to the Maxwell point from this general expression. The front speed is linear around the Maxwell point. In one-dimensional bistable non-variational systems, fronts can be motionless at a point in the parameter space, without the need for both equilibria to have equal energy [11], which allows an extension of the Maxwell point concept for systems without free energy. Even walls connecting two equivalent vectorial fields through spontaneous symmetry breaking can spread according to a given chirality of the vector field [12–14].

Analytical formulas or general behaviors are usually not reachable because to the nonlinear nature of fronts. Here, we reveal that near

* Corresponding author.
E-mail address: pedro.aguilera.r@ug.uchile.cl (P.J. Aguilera-Rojas).

https://doi.org/10.1016/j.chaos.2023.113241
Received 12 January 2023; Accepted 6 February 2023

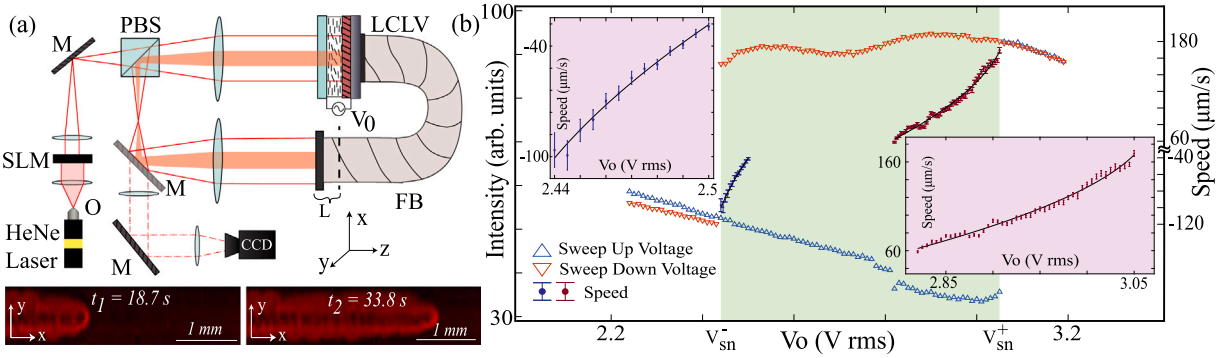

Fig. 1. Front propagation on a liquid crystal light valve (LCLV) with optical feedback close to the disappearance of bistability. (a) Schematic representation of LCLV with optical feedback setup. HeNe accounts for a Helium–Neon laser, SLM stands for the spatial light modulator, this device selects a quasi-1D region under static and uniform illumination, M are mirrors, PBS is the polarized beam splitter, V_0 is the driven voltage applied to LCLV, O is an optical objective, FB is a fiber bundle, CCD is a Charge-Coupled Device to monitor the LCLV evolution, and L accounts for the free propagation length. Lower panels show temporal snapshots sequence of the front propagation exhibited in the LCLV close to the disappearance of bistability. (b) Bifurcation diagram of the total intensity and front speed of the LCLV with optical feedback as a function of the voltage applied V_0 by $L = 0.0$ cm. The normal (△) and inverted (▽) triangles account for the total intensity of light measured by raising and lowering the voltage. The region of bistability is painted. V_{sn}^{+} accounts for the Fréedericksz voltage. The points with error bars account for the front speed between the different molecular orientations. Insets show a zoom of the front speed versus voltage V_0 near each bistability disappearance points. The continuous curves are the fits found for the front speeds, which have the form $v = v_0 + A\sqrt{|V_0 - V_{sn}^{\pm}|}$, where $\{v_0 = -183\ \mu m/s, A = 475.6\ V_{rms}^{-1/2}\ \mu m/s, V_{sn}^{-} = 2.41\ V_{rms}\}$, and $\{v_0 = 208.3\ \mu m/s, A = -292.3\ V_{rms}^{-1/2}\ \mu m/s, V_{sn}^{+} = 3.069\ V_{rms}\}$, for the left and right fit, respectively.

the disappearance of bistable fronts (transition between a bistable to a monostable region), the front speed follows a square root law as a function of the bifurcation parameter. Based on an experiment of a liquid crystal light valve with optical feedback, we characterize the law that describes the front speed near the disappearance of bistability. Theoretically, we consider different bistable models and show analytically and numerically that the front speed follows the aforementioned law. Our results apply both to systems that do or do not follow energy minimization principles. Experimental findings show a quite fair agreement with the theoretical results.

2. Experimental setup and results

A flexible experimental setup that exhibits multi-stability, front propagation, pattern formation, localized states, and spatiotemporal chaos is the liquid crystal light valve (LCLV) with optical feedback (see the review [15] and references therein). Fig. 1(a) shows a schematic representation of the LCLV with optical feedback. The LCLV consists of a nematic liquid crystal LC-654 (NIOPIK) with dielectric anisotropy constant $\epsilon_a = 10.7$ placed between two glass layers separated by a distance $d = 15\ \mu m$. Transparent indium tin oxide (ITO) electrodes and a photoconductive layer are deposed on the glasses to subject the liquid crystal to a driven voltage. A dielectric Bragg mirror with optimized reflectivity for 632.8 nm light is placed in the back layer of the liquid crystal cell. The LCLV can be electrically addressed by applying an oscillatory voltage V_0 rms and frequency $f_0 = 1.0$ kHz across the liquid crystal layer. In addition, the system is optically forced with a He–Ne laser ($\lambda_0 = 632.8$ nm). The LCLV is placed in a $4f$ optical configuration ($f = 25$ cm), as indicated in Fig. 1(a). The optical feedback circuit is closed with an optical fiber bundle (FB) placed at a distance $4f$ from the LCLV front face. The optical fiber bundle injects the light into the photoconductive layer, applying an additional voltage to the liquid crystal material depending on the light intensity. The feedback optical loop is designed so that light simultaneously presents diffraction propagation (characterized by the length L) and polarization interference induced by the polarizing beam splitter (PBS). A spatial light modulator (SLM, Holoeye LC 2012) is considered to carry out two-dimensional or one-dimensional experiments with different geometry. The SLM operates in transmit configuration and is a light amplitude modulator. In addition, the SLM can allow us to force the system periodically [9,16] or spatiotemporally [17].

When the cell is illuminated, the voltage applied to the liquid crystal cell V_0 is modified. In addition, as a consequence of optical feedback, the system exhibits a subcritical bifurcation characterized by two different molecular orientation states [15,18]. The Fréedericksz voltage characterizes the reorientation transition (see V_{sn}^{+} in Fig. 1b). Because of these molecular orientations have different refractive indices, each equilibrium has a different intensity (see snapshots in Fig. 1a). Using the SLM, we can induce different domain walls and study the fronts propagation (see the video in Supplementary material [19]). Most precisely, fronts are usually triggered by the edges of the area under study, quasi 1D channel induced by the SLM, or by local perturbations generated by SLM that increases or decreases the illumination inside the channel. The bistability region is bounded by $\{V_{sn}^{-}, V_{sn}^{+}\}$, where $V_{sn}^{\pm}$ account for the disappearance of the bistability points. We have measured the front speed between two stable states close to the disappearance of bistability. Fig. 1(b) summarizes the results found. From this chart, we conclude that the front speed close to the bistability disappearance exhibits a law of the form

$$v = v_0 + A\sqrt{|V_0 - V_{sn}^{\pm}|}, \tag{1}$$

where v_o is the front speed at the fold points. The main origin of the error bars and the initial propagation of front are the inherent fluctuations of the system (noise) and the heterogeneities of the experimental setup. To shed light on the origin of this law, we will now consider different bistability models and analyze the front propagation.

3. Front propagation in prototype bistable models

A simple model that accounts for the transition from disordered to oriented molecules state (nematic-isotropic transition) was proposed by De Gennes [20], which has the dimensionless form (the Landau-De Gennes model)

$$\partial_t u = \mu u + \alpha u^2 - u^3 + \partial_{xx} u, \tag{2}$$

where $u(x,t)$ is an order parameter, μ is the bifurcation parameter, α accounts for the nonlinear response. The last term accounts for elastic coupling, where ∂_{xx} is the Laplacian operator. The model Eq. (2) has also been used to describe hard colloidal rods [21], and anisotropic superfluid [22]. Eq. (2) has three trivial equilibria $u = u_0 \equiv 0$ and $u = u_{\pm} \equiv (\alpha \pm \sqrt{\alpha^2 + 4\mu})/2$. Fig. 2 shows the bifurcation diagram of Eq. (2). For $\mu < 0$, the u_0 state is stable, and for $\mu = \mu_T \equiv 0$, the system exhibits a transcritical instability, which generates that u_+ and u_- state are stable ones. The system is monostable when $\mu < \mu_{sn} \equiv -\alpha^2/4$, where the only stable equilibrium is u_0. The system is bistable for $\mu \geqslant \mu_{sn}$ (cf. Fig. 2). Namely, the system exhibits a transition from a bistable to

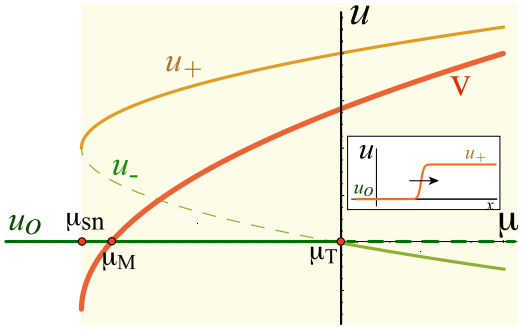

Fig. 2. Bifurcation diagram of Eq. (2). Equilibria u (u_0, u_-, and u_+) as a function of μ. The hard and dashed curves account for stable and unstable states respectively. The painted region stands for the bistable zone. The thick curve v stands for the front speed $v = \sqrt{2}(\alpha - 3\mu/u_+)/2$ between u_0 and u_+ state. μ_M accounts for the Maxwell point. The inset stands for a front profile.

a monostable region for $\mu = \mu_{sn}$ (disappearance of bistability). Then, the model presents a bistability region for $-\alpha^2/4 \leqslant \mu \leqslant 0$. Within this interval, the model Eq. (2) has fronts between u_0 and u_+ state, which has the form

$$u_F(x,t) = \frac{u_+}{2}\left[1 + \tanh\left(\frac{u_+(x - vt)}{2\sqrt{2}}\right)\right], \tag{3}$$

where $v = (\alpha - 3u_+/2)/\sqrt{2}$. This is one of a few examples where the front speed is known in the entire parameter space. Close to disappearance of bistability, $\mu = -\alpha^2/4 + \Delta\mu$ where $\Delta\mu$ is a small parameter ($\Delta\mu \ll 1$) and $u_+ \sim \alpha/2 + \sqrt{\Delta\mu}$, the front speed between to stable states takes the form $v = v_0 + A\sqrt{\Delta\mu}$ with $v_0 \equiv \alpha/4\sqrt{2}$ and $A \equiv -3/2\sqrt{2}$.

4. Generic variational reaction–diffusion model

In one-dimension dynamical systems, a general description of a bistable system is given by the reaction–diffusion equation, which reads

$$\partial_t u = -\frac{\partial V}{\partial u} + \partial_{xx} u, \tag{4}$$

where $u(x,t)$ is a variable that describes the system under study and $V(u)$ is a bistable potential. In the case that the potential describes a symmetric system (Allen–Cahn equation [23]), the above model describes the domain walls dynamics. Assuming that the system has two equilibria, $\mathcal{A}$ and $\mathcal{B}$, that is, $\partial V(\mathcal{A})/\partial u = \partial V(\mathcal{B})/\partial u = 0$. One expects the system to exhibit propagative fronts between these two equilibria of the form $u(x,t) = u_F(x - vt)$. Introducing this ansatz into the diffusion–reaction Eq. (4), multiplying by $\partial_x u$ and integrating over the whole space, after straightforward calculations, one obtains the speed of bistable fronts [8]

$$v = \frac{V(\mathcal{B}) - V(\mathcal{A})}{\int (\partial_x u)^2 dx}. \tag{5}$$

As we have mentioned, in case both states have the same energy, $V(\mathcal{A}) = V(\mathcal{B})$, the speed is zero.

Let us consider that equilibrium $\mathcal{B}$ is close to a saddle–node bifurcation (bistability disappearance), controlled by the bifurcation parameter Δ ($\Delta \ll 1$). Then $\mathcal{B} \approx \mathcal{B}_{sn} + \mathcal{B}_1\sqrt{\Delta}$ where $\mathcal{B}_{sn}$ is the equilibrium value at the bifurcation point. Since the front solution is proportional to the difference between equilibria, we can use $u(x,t) = (\mathcal{B} - \mathcal{A})H(x - vt)$. Using the above ansatz in formula (5), expanding in the Taylor series, one gets the universal law of front speed

$$v \approx \frac{V(\mathcal{B}_{sn}) - V(\mathcal{A})}{(\mathcal{B}_{sn} - \mathcal{A})^2 \int (\partial_x H_0)^2 dx}\left(1 - \frac{2\mathcal{B}_1\sqrt{\Delta}}{\mathcal{B}_{sn} - \mathcal{A}}\right), \tag{6}$$

$$\approx v_0 + A\sqrt{\Delta}, \tag{7}$$

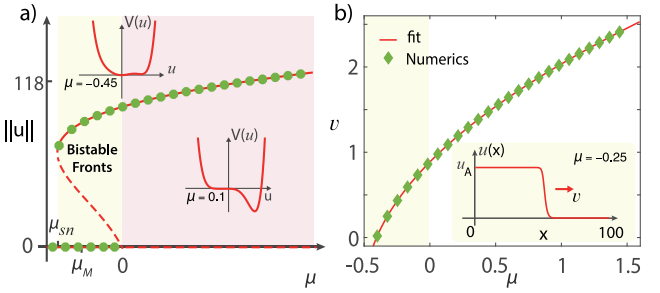

Fig. 3. Front propagation on the reaction–diffusion model (4) with cubic–quintic nonlinearity, $V(u) = -\mu u^2/2 - \beta u^3/3 - \delta u^4/4 + u^6/6$. (a) Bifurcation diagram, $\|u\| = \sqrt{\int u^2 dx}$ as a function of the bifurcation parameter μ with $\beta = 0.5$ and $\delta = 0.8$. The solid and dashed red curves are the analytical curve obtained by multiplying the equilibria by the length of the system. The insets show the potential in different regions of parameter space. The points show the results obtained numerically. (b) Front speed as a function of the bifurcation parameter μ. The diamonds (⋄) are the numerical results, and the continuous curve is the fit curve, formula (1), with $v_0 = -0.383$, $A = 1.971$, and $\mu_{sn} = 0.45$. Inset shows a typical profile of a front solution.

where v_0 is the front speed at the bistability disappearance point and $H_0 = H(x - v_0 t)$. Hence, any one-dimensional diffusion reaction-like system near the bistability disappearance will exhibit a square root-law front speed as a function of the bifurcation parameter. This is consistent with the experimental (see Fig. 1) and theoretical observations (cf. Fig. 2) discussed above.

To verify the validity of the universal formula (7), we consider the bistable cubic–quintic model with the potential $V(u) = -\mu u^2/2 - \beta u^3/3 - \delta u^4/4 + u^6/6$. This potential has been used to study the dynamics of molecular reorientation of optical valves with spatially modulated optical feedback [24]. Fig. 3 shows the bifurcation diagram of this model with cubic–quintic nonlinearity and the front speed as a function of the bifurcation parameter. Note that there is no analytical formula for the front speed in this model. Unexpectedly, the universal formula (1) describes the front speed quite well, even far from its validity region.

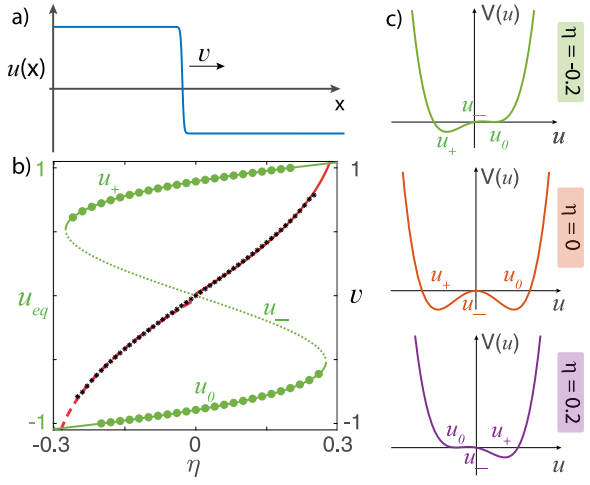

Fig. 4. Front propagation in the reaction–diffusion model (4) for a nascent bistability potential, $V(u) = -\eta u - \mu u^2 + u^4/4$. (a) Typical front profile. (b) Bifurcation diagram (green points and curves) and the front speed (black stars) as a function of the bifurcation parameter η with $\mu = 0.2$. The left and right vertical axes account for equilibria (u_{eq}) and the front speed, respectively. The solid and dashed curves are the stable (u_+, u_0) and unstable (u_-) states, respectively. The points show the results obtained numerically. The red solid ($v_0 = 1.358$, $A = -2.45$, and $\eta_{sn} = 0.3$) and dashed ($v_0 = -1.342$, $A = 2.401$, and $\eta_{sn} = 0.3$) curves are the fit curve formula (1). (c) The potential in different points of parameter space with $\mu = 0.8$. (For interpretation of the references to color in this figure legend, the reader is referred to the web version of this article.)

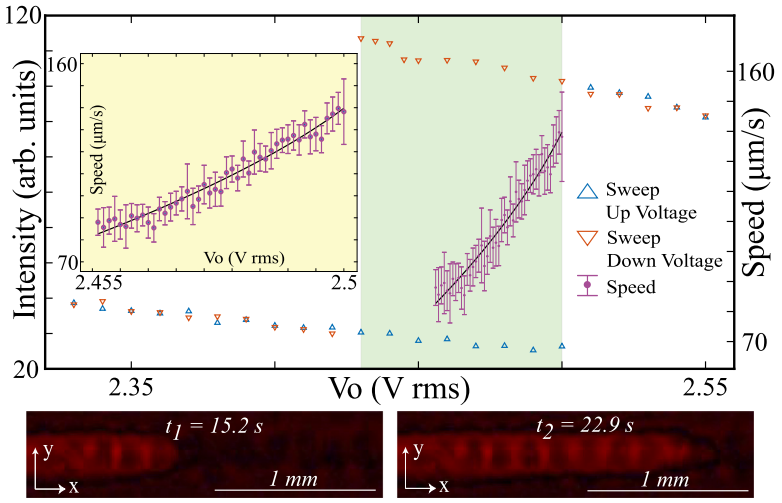

Fig. 5. Bifurcation diagram and front speed in a LCLV with free diffraction $L = -1.0$ cm and spatiotemporal optical feedback. This diagram is obtained using the same experimental setup as in Fig. 1a, where the SLM now fulfills a dual role, selecting the quasi-one-dimensional region and spatiotemporally modulating the illumination on the optical liquid crystal light valve. The diamonds and their respective error bars account for the front speed near the bistability disappearance. The solid line is obtained using fit (1) with $v_0 = 203.5$ μm/s, $A = -489.1\ V_{rms}^{-1/2}$ μm/s, and $V_{sn} = 2.517\ V_{rms}$. Insets account for a magnification of the front speed as a function of V_0. Lower panels show temporal snapshots sequence of the front propagation.

Another relevant bistable model used to describe the nascent of bistability [25] or an imperfect pitchfork bifurcation, is the one governed by equation Eq. (4) with $V(u) = -\eta u - \mu u^2 + u^4/4$. This type of reaction-diffusion equation has been used to explain chemical reactions, biological models, and optical systems [26,27]. Fig. 4 shows the bifurcation diagram for this potential, its respective bistability zone, the shape of the potential for different values of the η parameter, the profile of the observed fronts, and the front speed as a function of the bifurcation parameter. In this case, the bistability region is bounded by two critical points (saddle-node bifurcations). At each of these critical points, we find the universal law for the front speed Eq. (1).

5. Non-variational systems

The experimental and theoretical results presented above are valid for gradient or variational systems. Namely, the dynamics of these systems minimize a given free energy. However, one can consider nonvariational effects (such as nonlinear gradients or diffusions) and study how the front propagation is modified [11]. Let us consider the following prototype nonvariational bistable model [11,28]

$$\begin{aligned}\partial_t u &= \eta + \mu u - u^3 + \partial_{xx}u + c(\partial_x u)^2 + bu\partial_{xx}u,\\ &= -\frac{\partial V}{\partial u} + \partial_{xx}u + c(\partial_x u)^2 + bu\partial_{xx}u,\end{aligned} \tag{8}$$

where the last two terms account for nonlinear drift and diffusion. A similar model with a spatial instability (anti-diffusion) has been used to explain localized states with spatiotemporal chaos [29]. The model Eq. (8) describes the LCLV with free diffraction ($L \neq 0$) and spatiotemporal modulated forcing [17]. This experiment is achieved using the same setup shown in Fig. 1a, where the SLM now does a double role, selecting the one-dimensional region and spatiotemporally modulating the illumination in the optical liquid crystal light valve. Indeed, $c = b = 0$ when the experimental setup does not have free diffraction. Since the non-variational terms are proportional to the spatial derivatives, they do not modify the equilibria. Hence, the bifurcation diagram shown in Fig. 4 is still valid for the non-variational model (8). Considering the non-variational terms as perturbative terms ($c \sim b \ll 1$), using the strategy presented in [11], we can calculate how formula (6) is modified. Then, after straightforward calculations, we obtain the front speed between stable states close to disappearance of bistability

$$v \approx \frac{V(\mathcal{B}_{sn}) - V(\mathcal{A})}{(\mathcal{B}_{sn} - \mathcal{A})^2 \int (\partial_x H_0)^2 dx}\left(1 - \frac{2\mathcal{B}_1\sqrt{\Delta}}{\mathcal{B}_{sn} - \mathcal{A}}\right) +$$

$$(\mathcal{A} - \mathcal{B}_{sn})\frac{c\int(\partial_x H_0)^3 dx + b\int(H_0\partial_x H_0\partial_{xx}H_0)dx}{\int(\partial_x H_0)^2 dx}. \tag{9}$$

Therefore, in the variational case the front speed close to the bistability disappearance point also follows formula (1). To verify the validity of this result, experimentally, we introduce a standing wave type spatiotemporal forcing in the LCLV with optical feedback [17]. Fig. 5 shows the bifurcation diagram and the front speed of the LCLV in the presence of free diffraction and spatiotemporal optical feedback. We observe a quite good agreement with the theoretical finding from this chart. A video with the non-variational front propagation is shown in the supplementary material.

6. Conclusion

In conclusion, close to the transition between a bistable to a monostable region, we have shown that the front speed between stable states follows a square root law as a function of bifurcation parameter, independently the system is variational or not. The experimental findings show a fairly fair agreement with the theoretical results. In the case of other steady-state instabilities, the front speed may exhibit other critical exponents depending on the bifurcation parameters; for example, in a transcritical bifurcation, a linear law governs the front speed [30]. Because of the nonlinear nature of the fronts between bistable states, there are generally no analytical formulas for the front speed. Then the strategy of studying critical points or bifurcations (such as the Maxwell point or point of disappearance of bistability) allows for having universal behaviors for the front speed.

Declaration of competing interest

The authors declare that they have no known competing financial interests or personal relationships that could have appeared to influence the work reported in this paper.

Data availability

Data will be made available on request.

Acknowledgments

This work was funded by ANID–Millennium Science Initiative Program–ICN17_012. P.J.A.R and M.G.C. are thankful for financial support from the Fondecyt 1180903 project. K.A.B acknowledges to Proyecto Impulso URJC 2022 no M2978.

Appendix A. Supplementary data

Supplementary material related to this article can be found online at https://doi.org/10.1016/j.chaos.2023.113241.

References

[1] Pismen LM. Patterns and interfaces in dissipative dynamics. Berlin: Springer; 2006.
[2] Murray JD. Mathematical biology I and II. New York: Springer-Verlag; 2001.
[3] Cross M, Greenside H. Pattern formation and dynamics in nonequilibrium systems. New York: Cambridge University Press; 2009.
[4] Langer JS. Instabilities and pattern formation in crystal growth. Rev Modern Phys 1980;52:1.
[5] Van Saarloos W. Front propagation into unstable states. Phys Rep 2003;29:386.
[6] Mendez V, Fedotov S, Horsthemke W. Reaction-transport systems: Mesoscopic foundations, fronts, and spatial instabilities. Berlin: Springer-Verlag; 2010.
[7] Castillo-Pinto C, Clerc MG, González-Cortés G. Extended stable equilibrium invaded by an unstable state. Sci Rep 2019;9:15096.
[8] Pomeau Y. Front motion, metastability and subcritical bifurcations in hydrodynamics. Physica D 1986;23:3.
[9] Haudin F, Elías RG, Rojas RG, Bortolozzo U, Clerc MG, Residori S. Driven front propagation in 1D spatially periodic media. Phys Rev Lett 2009;103:128003.
[10] Goldstein RE, Gunaratne GH, Gil L, Coullet P. Hydrodynamic and interfacial patterns with broken space–time symmetry. Phys Rev A 1991;43:6700.
[11] Alvarez-Socorro AJ, Clerc MG, González-Cortés G, Wilson M. Nonvariational mechanism of front propagation: Theory and experiments. Phys Rev E 2017;95:010202(R).
[12] Coullet P, Lega J, Houchmanzadeh B, Lajzerowicz J. Breaking chirality in nonequilibrium systems. Phys Rev Lett 1990;65:1352.
[13] Clerc MG, Coulibaly S, Laroze D. Nonvariational ising-Bloch transition in parametrically driven systems. Int J Bifurcation Chaos Appl Sci Eng 2009;19:2717.
[14] Michaelis D, Peschel U, Lederer F, Skryabin DV, Firth WJ. Universal criterion and amplitude equation for a nonequilibrium Ising-Bloch transition. Phys Rev E 2001;63:066602.
[15] Residori S. Patterns, fronts and structures in a liquid-crystal-light-valve with optical feedback. Phys Rep 2005;416:201.
[16] Alfaro-Bittner K, Castillo-Pinto C, Clerc MG, Gonzalez-Cortes G, Rojas RG, Wilson M. Front propagation into an unstable state in a forced medium: Experiments and theory. Phys Rev E 2018;98:050201(R).
[17] Aguilera-Rojas PJ, Clerc MG, Gonzalez-Cortes G, Jara-Schulz G. Localized standing waves induced by spatiotemporal forcing. Phys Rev E 2021;104:044209.
[18] Clerc MG, Residori S, Riera C. First-order Freedericksz transition in the presence of a light driven feedback. Phys Rev E 2001;63:060701.
[19] See Supplemental Material at for a movie that show the front propagation with zero ($L = 0.0cm$) and non zero ($L = -1.0cm$) diffraction length (Video 1).
[20] de Gennes PG, Prost J. The Physics of Liquid Crystals. 2nd ed.. Oxford: Oxford Science Publications, Clarendon Press; 1993.
[21] Everts JC, Punter MTJJM, Samin S, van der Schoot PPAM, van Roij R. A Landau-de Gennes theory for hard colloidal rods: Defects and tactoids. J Chem Phys 2016;144:194901.
[22] Ambegaokar V, deGennes PG, Rainer D. Landau-Ginsburg equations for an anisotropic superfluid phys. Rev. A 1974;9:2676.
[23] Allen SM, Cahn JW. A microscopic theory for antiphase boundary motion and its application to antiphase domain coarsening. Acta Metall 1979;27:1085.
[24] Alfaro-Bittner K, Castillo-Pinto C, Clerc MG, González-Cortés G, Jara-Schulz G, Rojas RG. Front propagation steered by a high-wavenumber modulation: Theory and experiments. Chaos 2020;30:053138.
[25] Tlidi M, Mandel P, Lefever R. Localized structures and localized patterns in optical bistability. Phys Rev Lett 1994;73:640.
[26] Kozyreff G, Tlidi M. Nonvariational real Swift-Hohenberg equation for biological, chemical, and optical systems. Chaos 2007;17:037103.
[27] Clerc MG, Petrossian A, Residori S. Bouncing localized structures in a liquid-crystal light-valve experiment. Phys Rev E 2005;71:015205.
[28] Alvarez-Socorro AJ, Castillo-Pinto C, Clerc MG, Gonzales-Cortes G, Wilson M. Front propagation transition induced by diffraction in a liquid crystal light valve. Opt Express 2019;27:12391.
[29] Verschueren N, Bortolozzo U, Clerc MG, Residori S. Spatiotemporal chaotic localized state in liquid crystal light valve experiments with optical feedback. Phys Rev Lett 2013;110:104101.
[30] Benguria RD, Depassier MC. Speed of fronts of the reaction-diffusion equation. Phys Rev Lett 1996;77:1171.